FREEDM SYSTEMS CENTER

Powertrain Electric Machines and Controls

FREEDM Annual Symposium

February 10, 2026

Presentation Overview

Electric Machines for Traction Applications

Electric Machines for UAV Applications

Model Free Predictive Control for IPMSM and Multi Active Bridge XFC

Q&A

Electric Vehicle Electric Machines

Design Trends: Increase DC-link Voltage and Machine Speed

High Pole Design
- Increases torque density
- Reduces end turn length
- Reduces cost of PMs

High Speed Design
- Increases power density
- Reduces system mass

Adoption of Hairpin Winding
- Increases efficiency
- Improves torque-density
- Improves overload capability

Adoption of DHD Winding
- Suffers at low speed efficiency
- Increases high speed efficiency
- Lower cost compared to hairpin
- Similar fill factor as hairpin

$(P_{den} \uparrow)$
$(T_{den} \uparrow)$

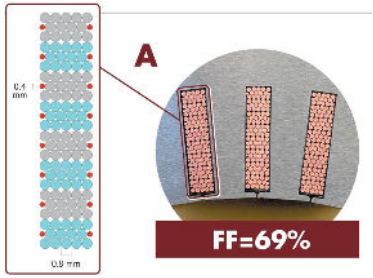

DHD winding

Hairpin winding

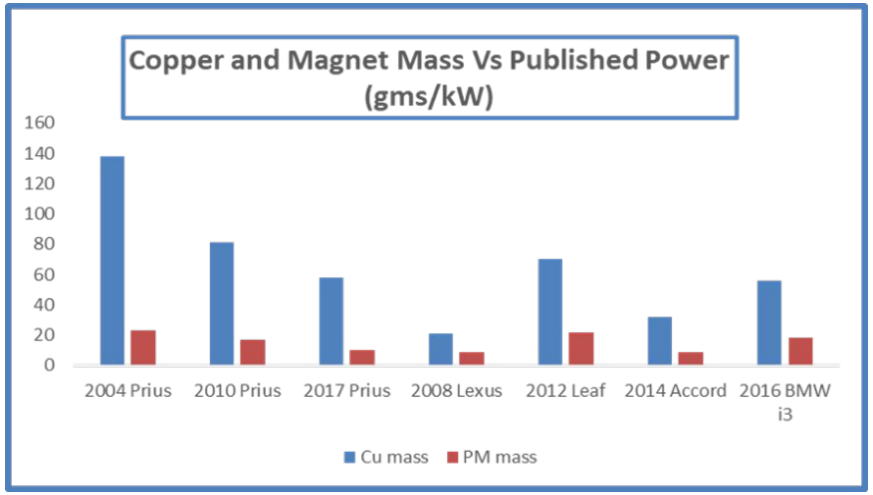

Wide Band Gap (WBG) Drives
- System power density increase
- Better current regulation
- System efficiency increase

*DHD - Distributed High Density Winding

Rugged 50kW/L Traction Electric Machine Designs

Sponsored by DOE-VTO Electric Drivetrain Consortium

FREEDM SYSTEMS CENTER

NC STATE UNIVERSITY

Design-I: Space-Shifted Asymmetrical Dual Three Phase IPM Synchronous Machine

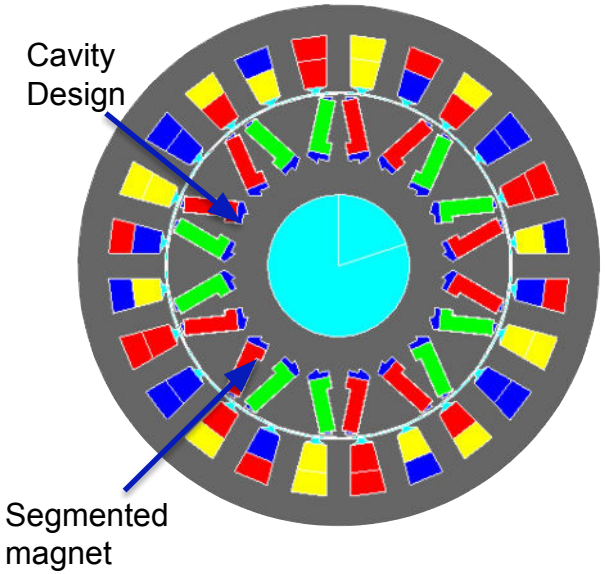

Parameters	Design I	Design II
Peak Torque for 15s (Nm)	145	144
Peak Power for 15s (kW)	100	100
Max. speed (rpm)	20,000	20,000
Power density (kW/L)	50	50

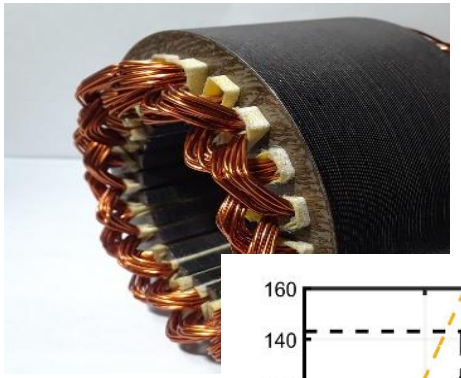

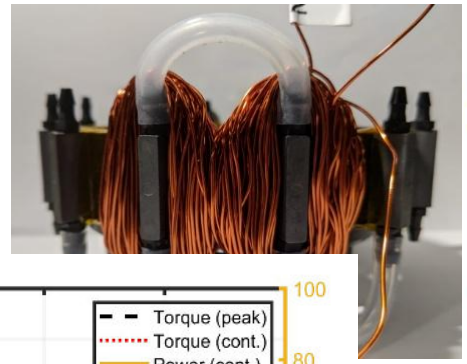

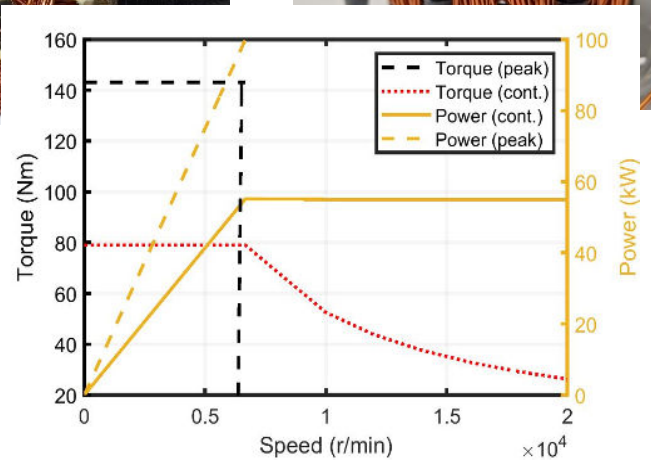

Target Torque Speed Profile

Design II: Slotless-Halbach PMSM with integrated in-teeth cooling

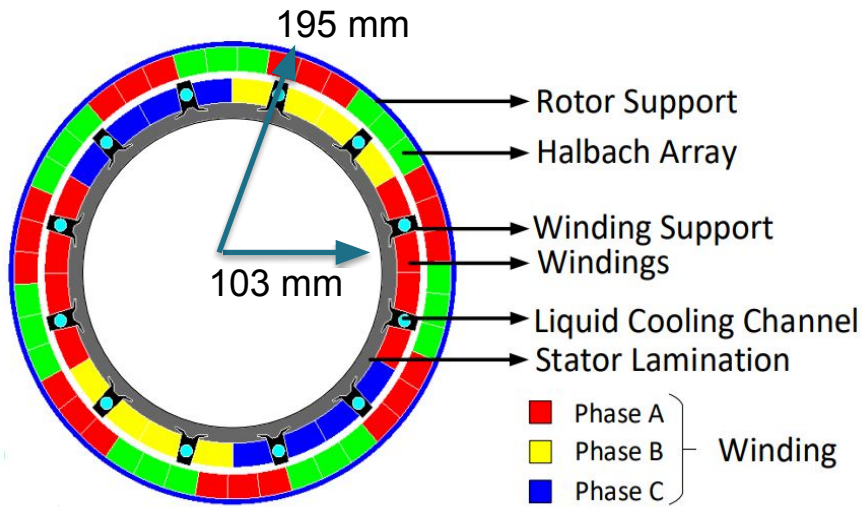

Design I Features:

- Dual Space-shifted wye-delta winding
- Segmented magnet and rotor design
- End winding potting with CoolTherm SC-320
- Hiperco 50 steel laminations

Design II Features:

- Multi-segment halbach array
- Slotless stator made from Coolpoly D5506 thermally conductive plastic
- Winding embedded liquid cooling

- M. S. Islam, M. A. Kabir and I. Husain, AC Machine Windings, US patent, 2019/0379251 A1, Issued Dec. 12, 2019.
- Md S. Islam, M. A. Kabir, R. Mikail and I. Husain, "Space-shifted Wye-Delta Winding to Minimize Space Harmonics of Fractional Slot Winding," in *IEEE Transactions on IA, 2020, Vol: 56, Issue: 3.*
- Md S. Islam, I. Husain and G. Buckner, 3D Airgap Slotless Permanent Magnet Electric Machine, Invention disclosure filed 27 Jan 2020.
- R. Chattopadhyay, Md S. Islam, R. Mikail and I.Husain, “Integrated In-teeth Cooling for High Power Density Slotless Motor,” 2020 IEEE ECCE.

Fabrication of 100kW SS-ADTP IPMSM: Rotor Production and Motor Assembly

- Rotor stack is made of 0.01” HF10 laminates bonded with EB-548 and cured under high heat and pressure.
- The SmCo magnets are bonded with a high-temperature adhesive and do not need any extra coating.
- The magnets are magnetized before insertion in the rotor stack.
- The splined shaft is inserted in the rotor cavity and the rotor stack is tightened by two steel plates at both ends.
- The completed rotor is subjected to a balancing process for even weight distribution.
- The balanced rotor is mounted on the front cover plate and centered in the airgap by a guide lock.
- A wave spring washer is placed on the bearings to absorb stress and reduce mechanical vibrations.

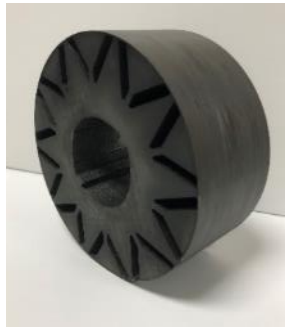

HF-10 rotor lamination stack

Segmented SmCo magnets

Magnet insertion with adhesive

Rotor mounting

Completed ADTP IPMSM

Experiment Test Setup

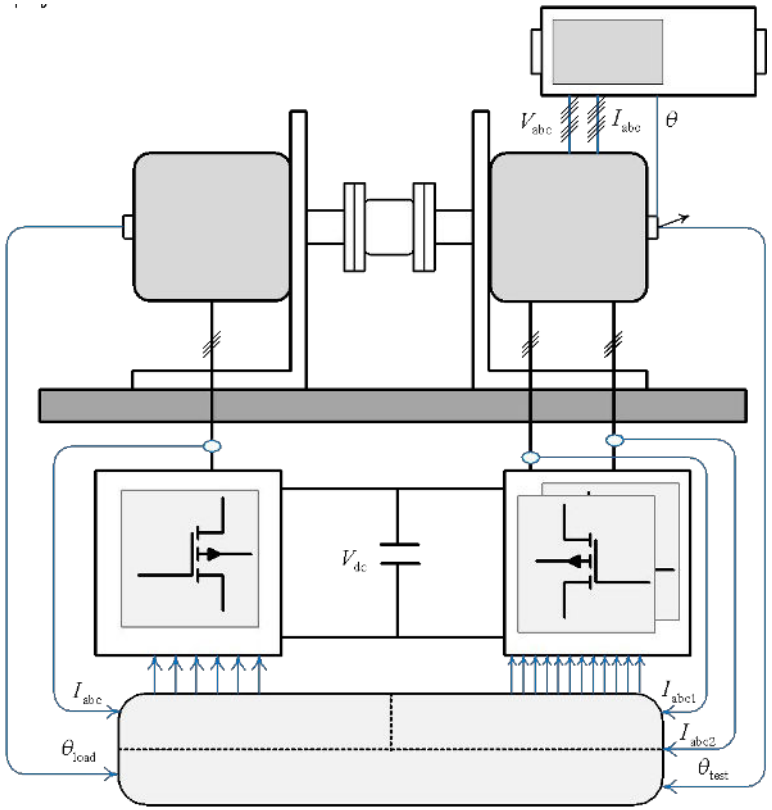

Schematic diagram of Experiment Test Setup

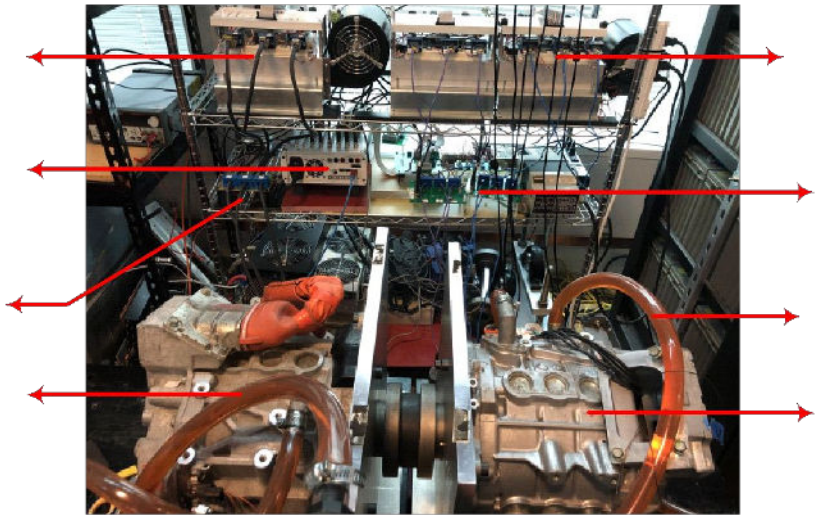

Dynamometer Test Stand

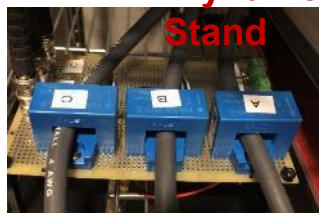

Current Sensors

dSPACE MicrolabBox

DC Power Supply

Power Analyzer

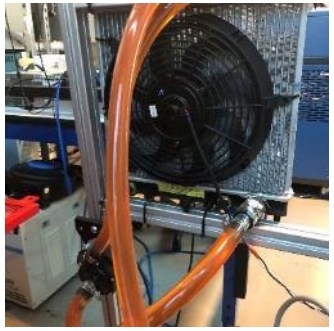

Radiator and Water Pump

SS ADTP IPMSM No Load Test Results

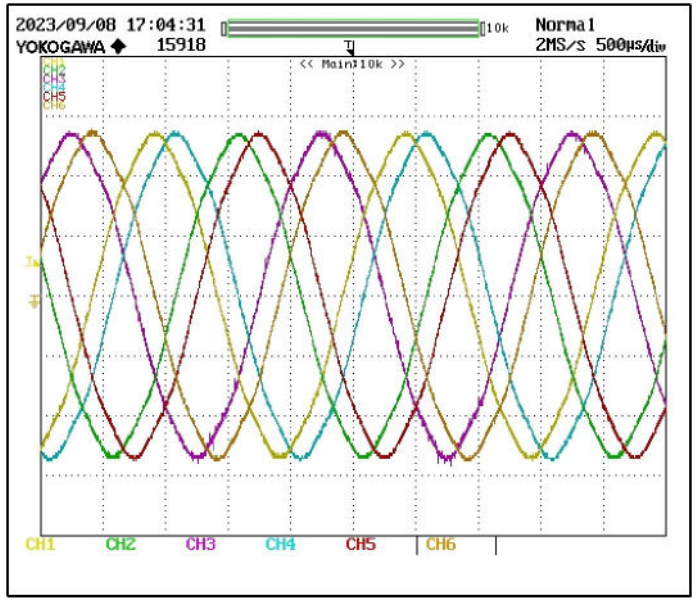

Line back EMF waveform at 6,000 r/min

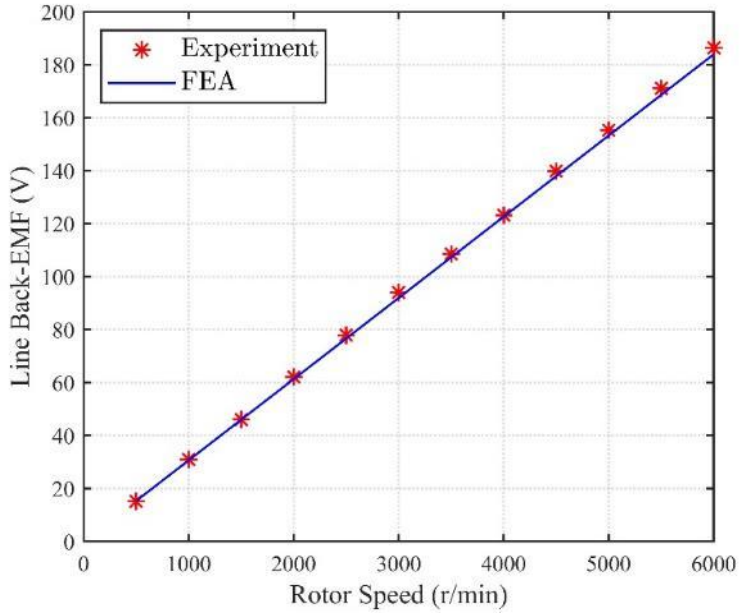

Comparison of RMS value Line back EMF with FEA predictions

- Line-Line resistance at room temperature = 110 mΩ
- The measured line back EMF waveforms are balanced and have the correct phase shift.
- The 5^{th} and 7^{th} order harmonic components of the line back EMF are only 1.5% and 1.1% of the fundamental at 6,000 r/min.
- The rms values of the back EMF are in good agreement with FEA predictions.
- The back emf constant/rotor flux = 47.7 mWb.
- The 8-pole EM61 resolver is recalibrated for the 10-pole IPMSM prototype.

SS-ADTP IPMSM Torque Control Test Results

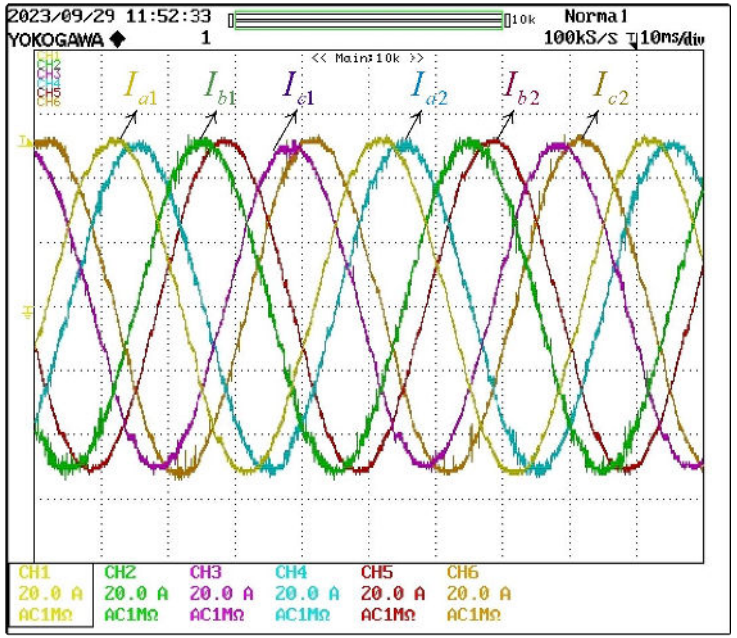

Steady-state phase current waveform at a load of 52 A

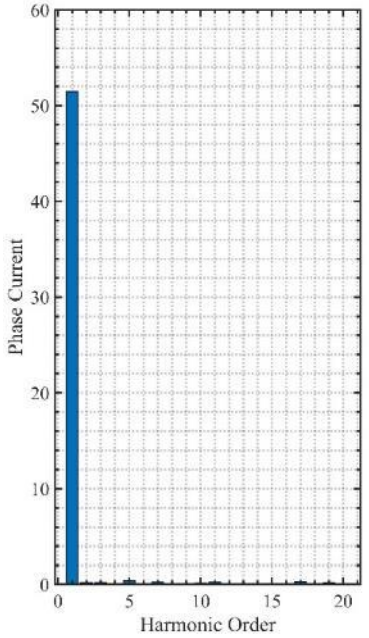

Harmonic spectrum of phase A1

- The PI controller gains are first calculated from design rules based on pole-zero cancellation and later refined by a trial-and-error tuning process
- The 3rd, 5th, and 7th harmonic components are less than 0.5% of a 52 A fundamental load current.
- The dq currents track their references and the harmonic currents and zero sequence currents are suppressed to zero.

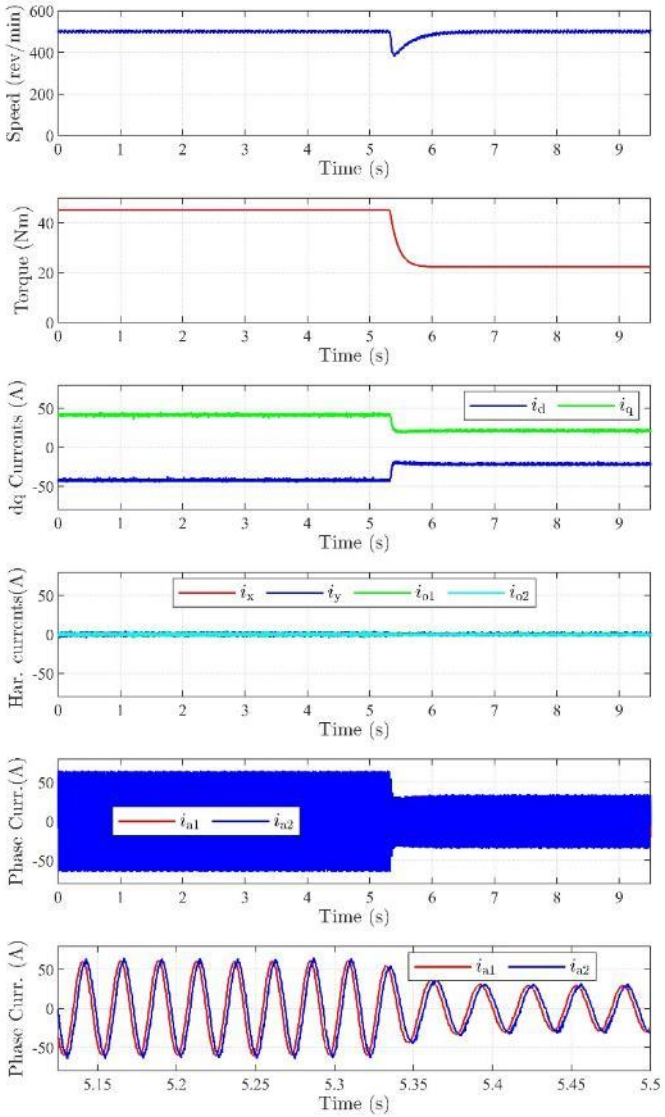

Dynamic response under a step change from 60A to 30A at a control

100 kW Segmented Rotor-Wound Field Synchronous Machine

- 100 Nm, 52 kW, segmented rotor WFSM (SR-WFSM) designed and optimized to maximize saliency ratio
- 36 slot/6 pole configuration; rotor consists of six laminated segments mounted on a non-magnetic sleeve
- Shape of cavity between segments obtained through optimization
- Laminations made from B20AV1200 steel (0.2 mm laminations).
- Rotor sleeve fabricated from aluminum with 30 mm shaft dia.
- Assembly complete; Testing in progress

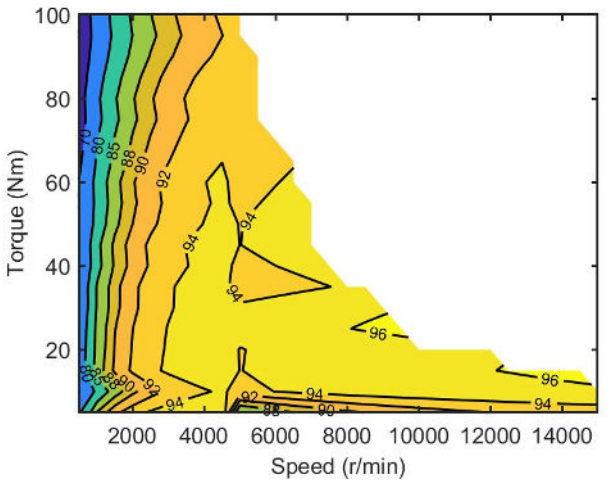

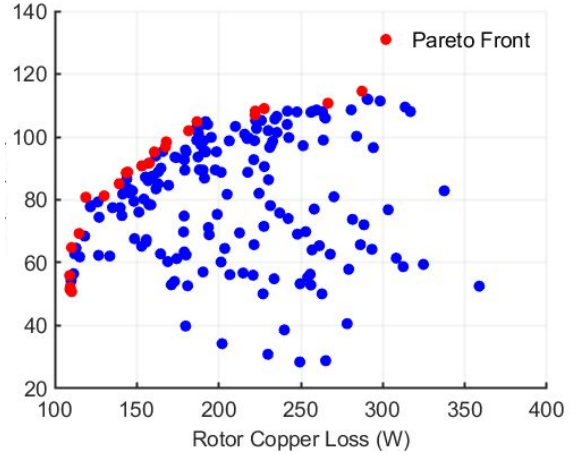

Efficiency map of Segmented WFSM

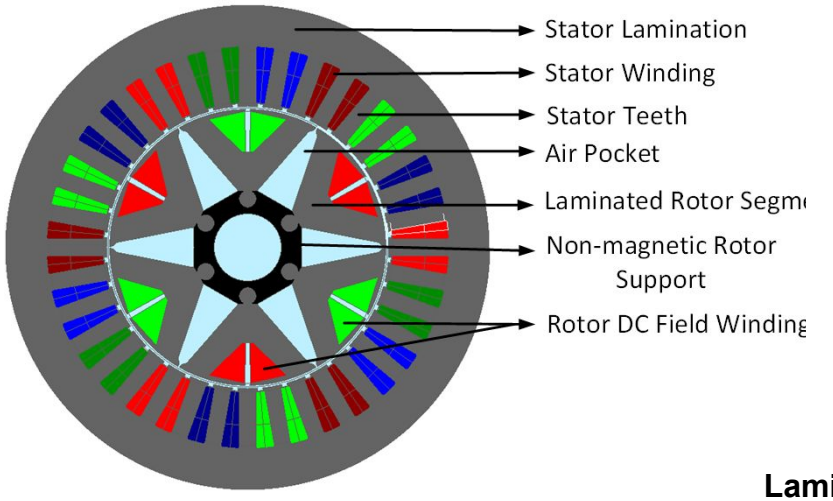

Laminated rotor pole segment

Rotor sleeve/ lamination holder

Assembled rotor

Stator laminations

Assembly of WFSM

- Assembly of the WFSM is currently ongoing.
- The shaft is being made to accurately hold the rotor and slip ring in place.
- Nissan leaf EM61 motor housing frame used
- The housing frame is extended to accommodate the slip ring.
- Expected completion by the end of February.

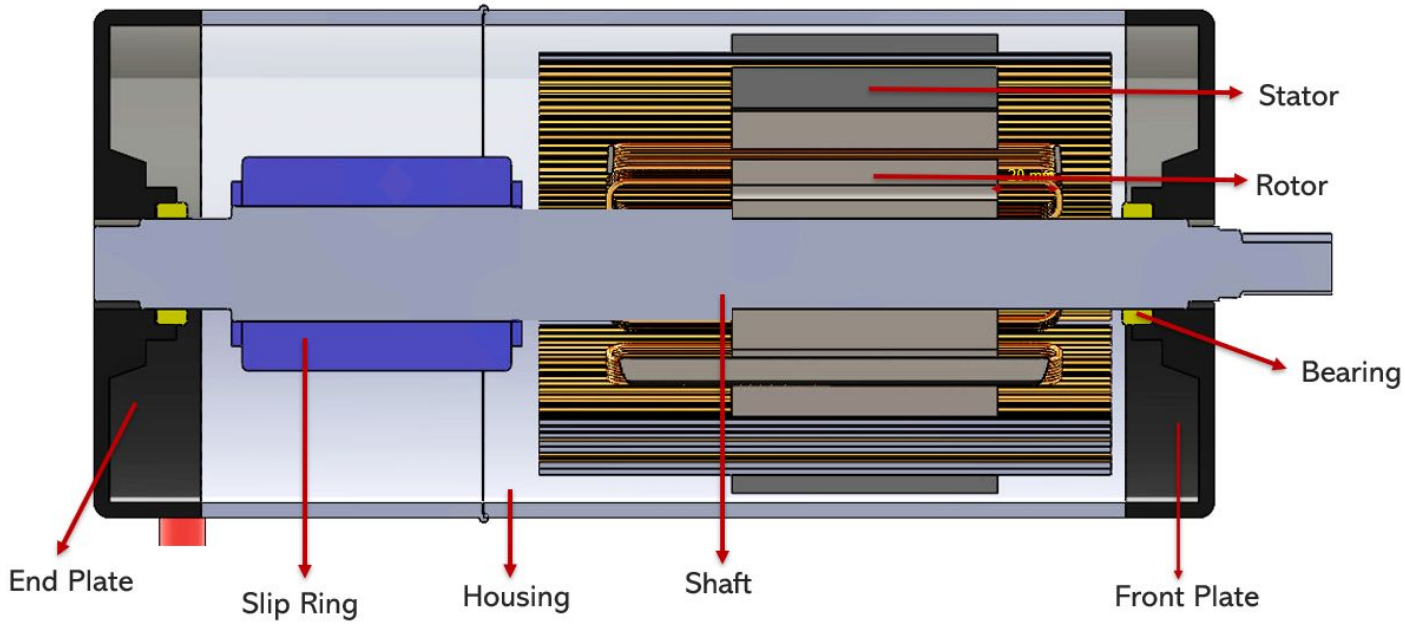

Cross Section of the Proposed Motor Assembly

Stator Housing

Completed Stator

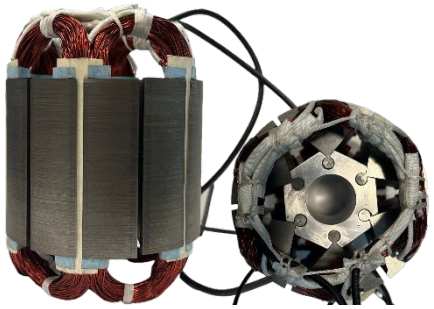

Completed Rotor

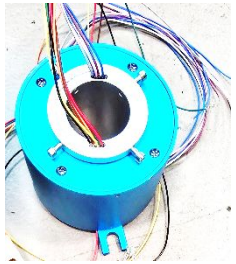

Slip Ring

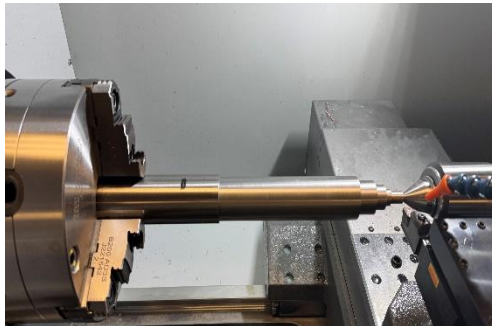

Shaft being fabricated

Asymmetric Dual Three Phase Slotless Hybrid Flux Motor (ADTP-HFM) for Traction Applications

- Hybrid Flux Motor integrates radial and axial topologies in one geometric structure.
  - Utilizes the structural and inactive components for torque production
  - Improves torque density
- Asymmetric dual three phase improves torque and ensures reliable operation during 3-ph fault.
- Non-magnetic teeth/winding support in slotless motor configuration
  - Low coreloss
  - Low torque ripple
  - The nonmagnetic stator teeth can be used for a motor cooling mechanism, such as Winding Embedded Liquid Cooling (WELC)

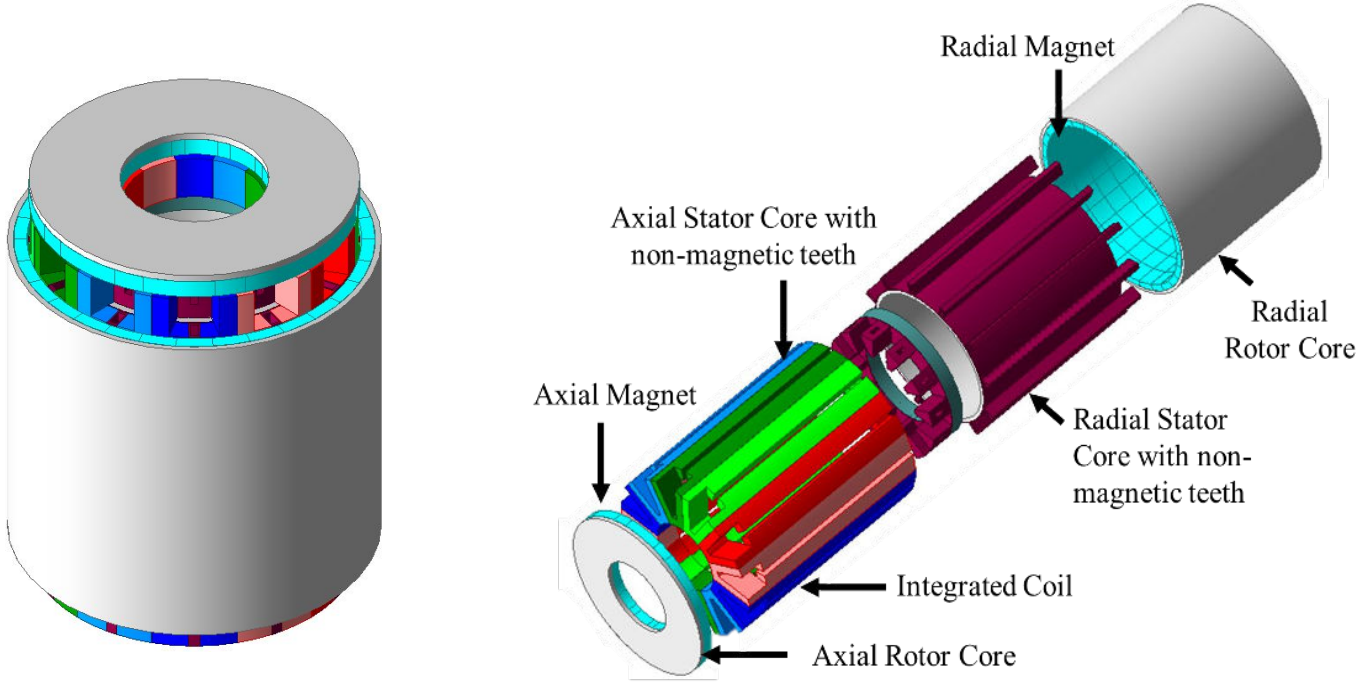

Fig. ADTP-HFM (a) Assembled view (b) Exploded View

M. J. Al Hossain, J. Jung, M. S. Islam and I. Husain, "Electromagnetic Design and Analysis of an Asymmetric Dual Three Phase Slotless 3D Airgap Electric Machine for High Power Density Applications," 2025 IEEE International Electric Machines & Drives Conference (IEMDC), Houston, TX, USA, 2025, pp. 879-885,

Asymmetric Dual Three Phase Slotless Hybrid Flux Motor (ADTP-HFM) for Traction Applications

- Hybrid Flux Motor follows the superposition principle for torque and back EMF (T & BE)
  - Hybrid Flux = Radial Flux + Axial Flux
    T & BE T & BE T & BE
  - Radial and axial motors can be designed and optimized independently and then integrate.
  - Reduced computation time

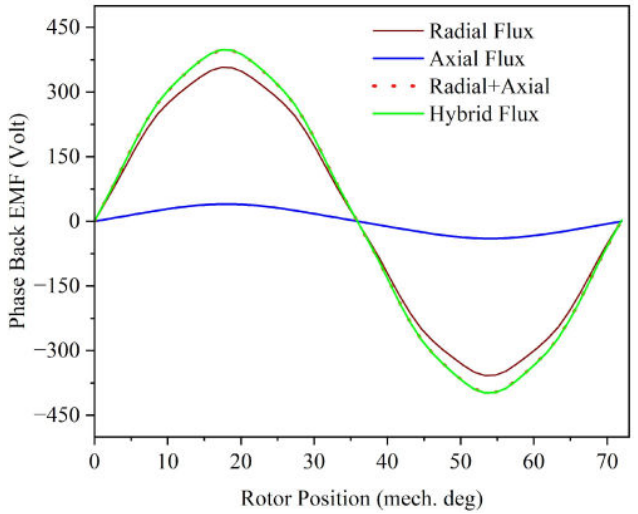

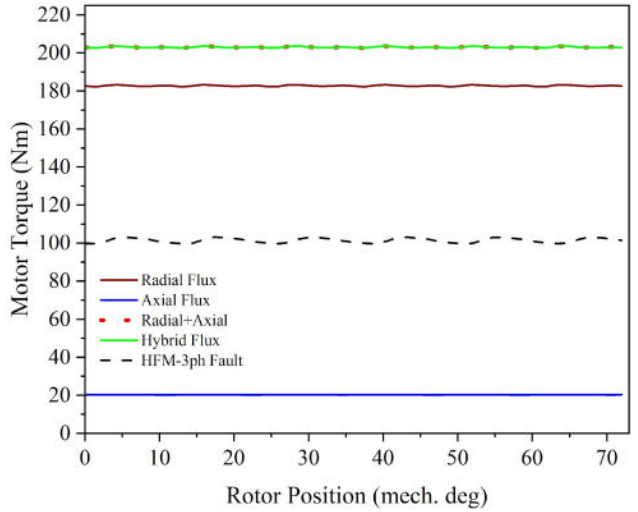

- Winding Embedded Liquid Cooling enables the hybrid flux motor to operate with high current density.
  - Cooling channels along the winding teeth/support provide low thermal resistance path from heat source (winding) to heat sink (Cooling channel)
  - Significantly improves thermal performance

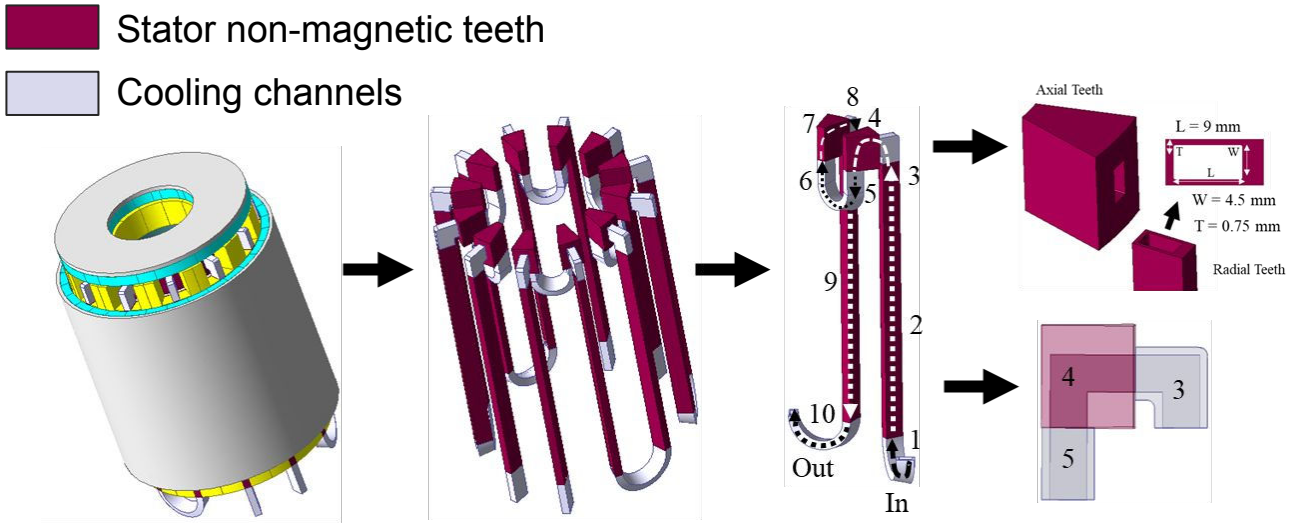

Flow Direction: In >1 > 2 > 3 > 4 > 5 > 6 > 7 > 8 > 9 >10> Out

Axial Flux Machine with Ceramic Windings

Thermal Advantage of Ceramic Substrates

- In conventional and PCB windings, copper is surrounded by thermally insulating materials
- This leads to heat pooling and hotspots in copper, which limits the maximum current density.
- In AMB windings, path from conductor to coolant/ambient air is comprised of thermally conductive materials, allowing much higher current density. This allows usage of lower copper volume.

Dual-Rotor Axial Flux Machine with Ceramic Windings

- Stator coils mounted on 3D printed coil holders which are fastened onto the endplate
- Each 40 pole rotor comprises of 40 N42 NdFeB magnets.
- N-S alignment of rotors eliminates necessity of stator core
- Airgap of 2 mm, entire stator (substrate + copper) has axial thickness (l_g) of 1.24 mm.

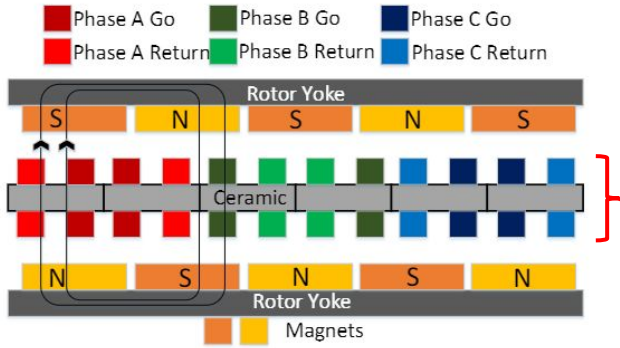

Electromagnetic schematic of CS-CAFM

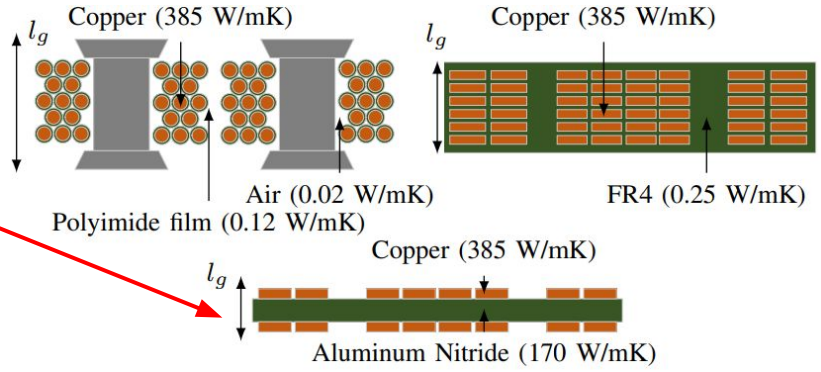

Thermal schematic of various axial flux coreless stators

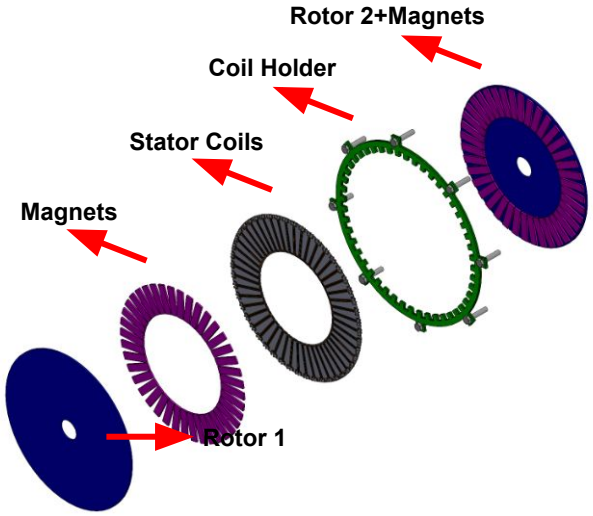

Exploded view of dual rotor CS-CAFM

Axial Flux Machine with Ceramic Windings

- Prototype machine with 0.3 mm copper on 0.635 mm AlN substrate (AMB) fabricated.
- Stator comprises of 8 coil groups, each comprising of 6 coils.
- End connections made using external wires to form 40 pole winding.

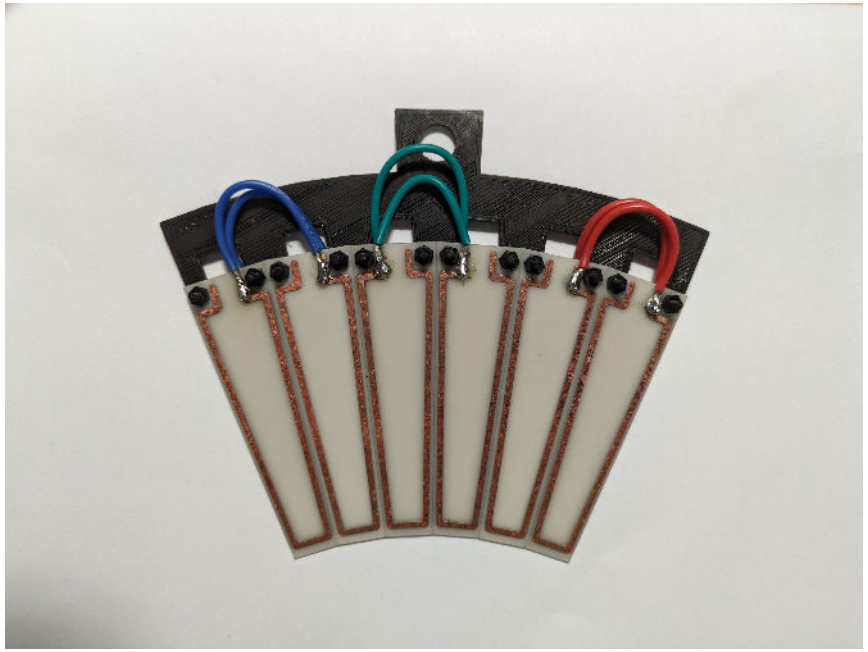

Coils of three phases forming a pole

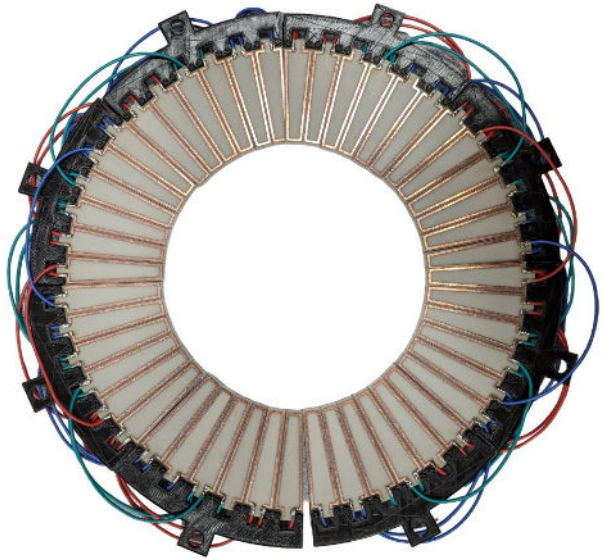

Complete stator winding before final assembly

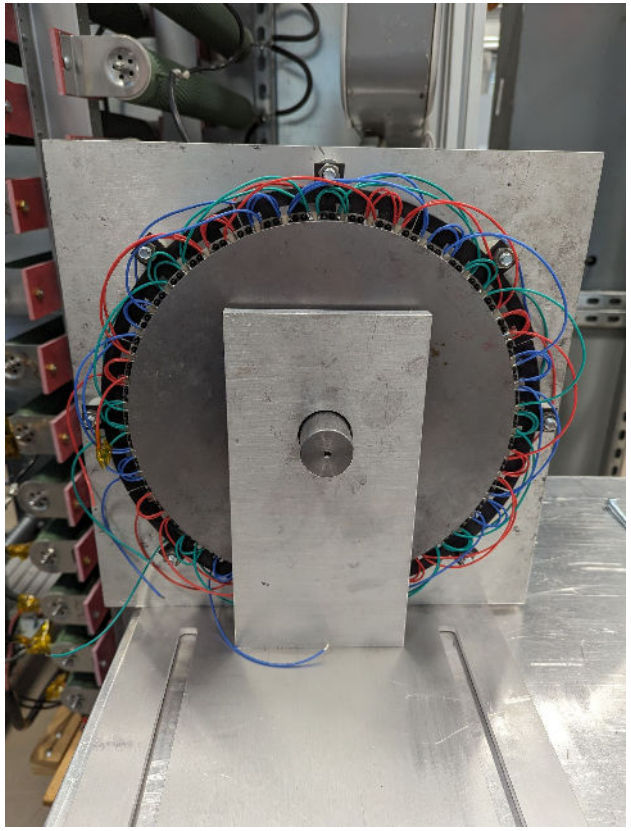

Assembled motor with one rotor and stator coils visible

AMB Axial Flux Machine Experimental Results

- Maximum continuous current density or an 80 °C rise in temperature, obtained from a thermal test on one 2-sample coil is 28 A/mm^2 (12.5 A).
- For a current density of 56 A/mm^2 (25 A), peak transient duration was:
  - 30 seconds for natural convection
  - 41 seconds for forced convection (crossflow)
- CS-CAFM tested in 10 HP dynamometer setup
- Open circuit tests performed to obtain variation of back-emf with speed and three-phase back-EMF waveforms.

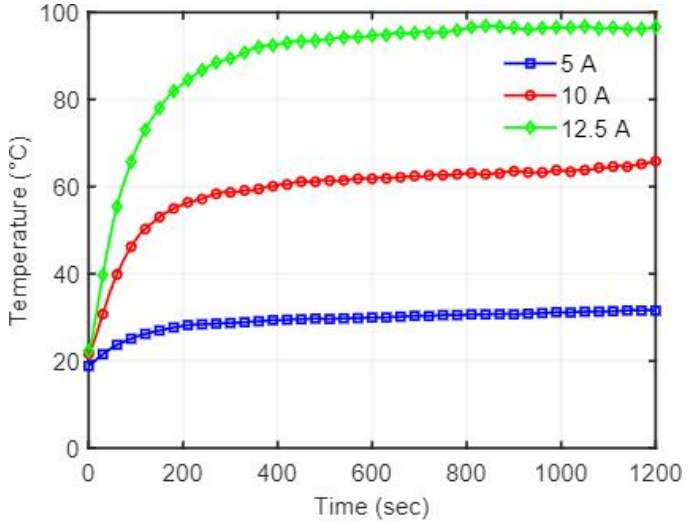

Temperature rise for continuous operation

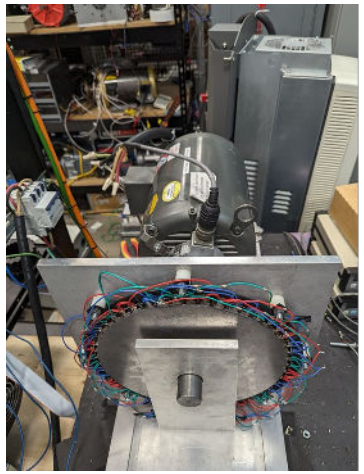

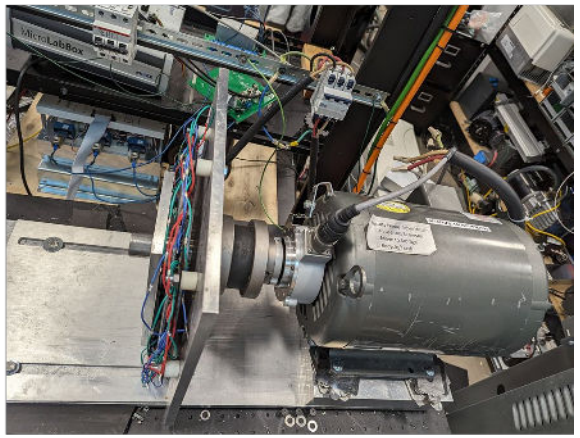

Dynamometer test setup for CS-CAFM prototype testing

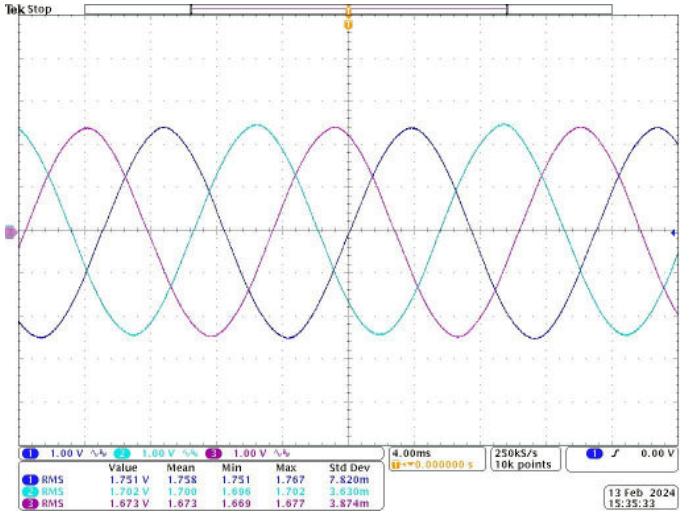

Experimental 3-ϕ Back-EMF at 200 r/min

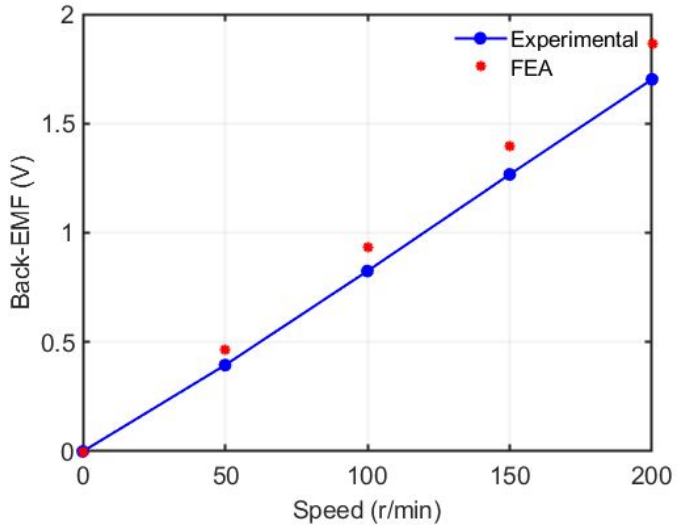

Back-EMF variation with speed

Lightweight UAV Motor

Development of a UAV-Based Medical Supply System for Rapid Response to Healthcare Crises in Rural Areas (DOE-NIST project)

- High torque and mass/loss reduction is beneficial for UAV propulsion motors
- High pole count/high fundamental frequency => high core loss
- Using ferrite (low loss, low mass density, low B_{sat}) for stator back yoke and Hiperco (low loss, high mass density, high B_{sat}), light weight, high efficiency at light load condition is achievable
- To compensate mass increase due to Hiperco, aluminum (low mass density, high resistivity) winding is used

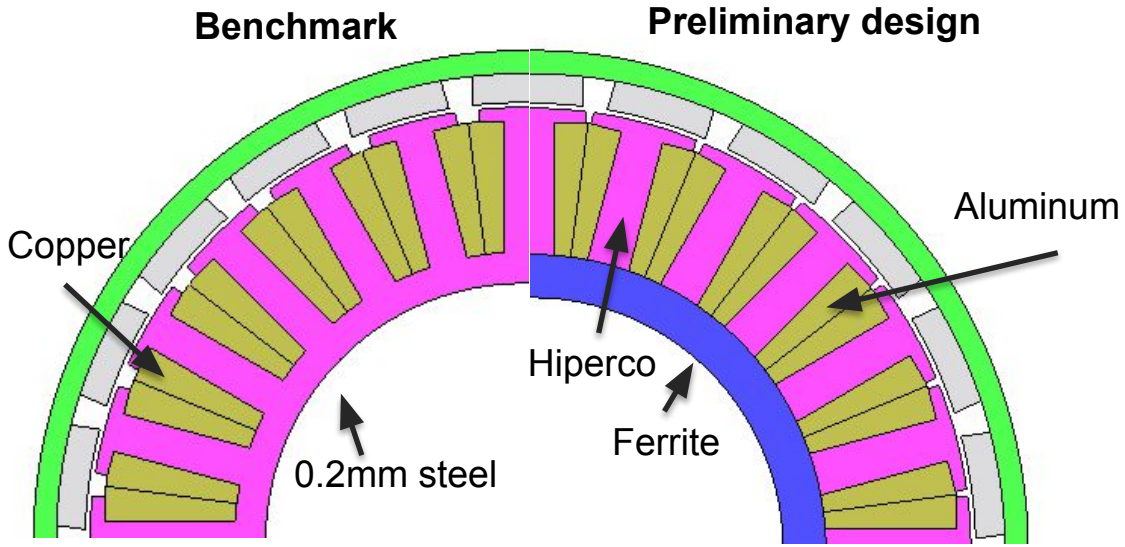

	Benchmark	Pre. Design
Teeth	0.2mm Steel	Hiperco
Yoke	0.2mm Steel	Ferrite
Winding	Copper	Aluminum
Slot Fill	0.33	0.55
Stator Mass [g]	244	201.5
Average torque [Nm]	1.08	
Speed [rpm]	5557	
Winding loss [W]	25.9	24.6
Core loss, teeth [W]	28.8	27.1
Core loss, yoke [W]	5.6	0.0
PM loss [W]	3.7	1.8
Rotor loss [W]	4.4	1.5
Total EM loss [W]	68.4	55.1
Mechanical loss [W]	48.5	48.5
Efficiency	84.3%	85.8%
Torque ripple [%]	16%	17%
	224	188

Ferrite Core Prototype Design

- For proof of concept, instead of using custom made ferrite core, off-the-shelf ferrite core is used
- 0.2mm electrical steel is used instead of Hiperco
- Due to the small ferrite core size, stator teeth size is increased => mass and core loss increase

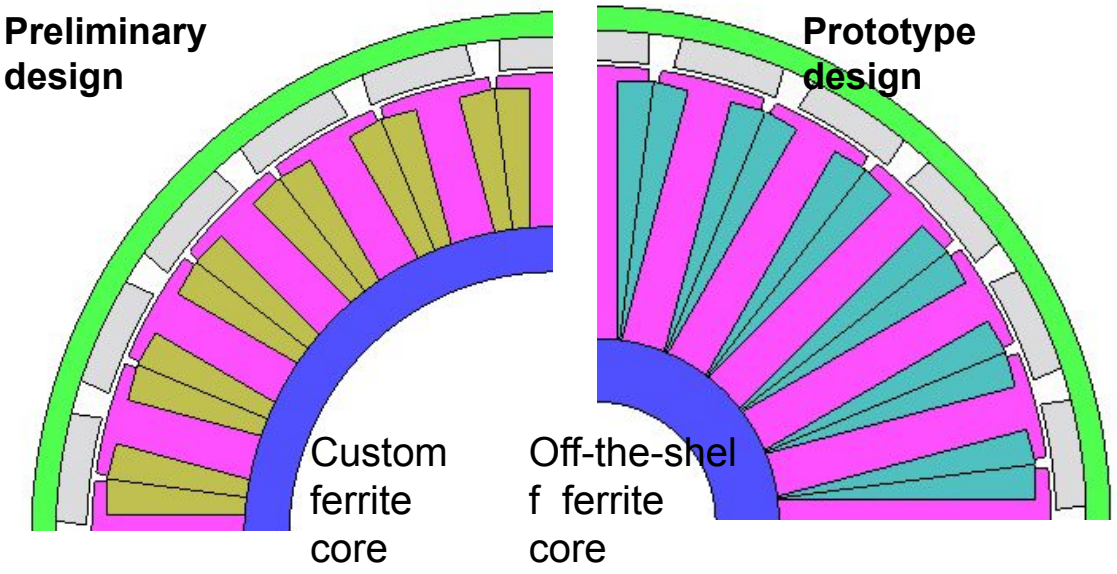

	Pre. Design	Proto. Design
Teeth	Hiperco	0.2mm steel
Yoke	Custom ferrite	Off-the-shelf ferrite
Winding	Aluminum	Aluminum
Slot Fill	0.55	0.55
Stator Mass [g]	201.5	281
Average torque [Nm]	1.08	
Speed [rpm]	5557	
Winding loss [W]	24.6	21.2
Core loss, teeth [W]	27.1	38.1
Core loss, yoke [W]	0.0	0
PM loss [W]	1.8	1.3
Rotor loss [W]	1.5	1.4
Total EM loss [W]	55.1	62.1
Mechanical loss [W]	48.5	48.5
Efficiency	85.8%	85.0%
Torque ripple [%]	17%	15%
	188	188

Ferrite Core Motor Test Result

- Measured values are close to the design values from FEM and analytical calculation
- Due to the limited manufacturing capability, slot fill factor achieved is 37%
- With proper manufacturing, slot fill factor of 55%, $R_{ph} = 9.54m\Omega$
- Thrust/loss was measured up to 5000rpm with a 20 x 10 propeller
- The lower the motor input power, the higher efficiency
- If manufactured properly, the ferrite core motor can have high efficiency at light load operating condition

	FEM/ANA	Meas.	Err.
Back-emf @1498rpm	3.45V	3.31V	-4.2%
			-3.2%
			3.1%

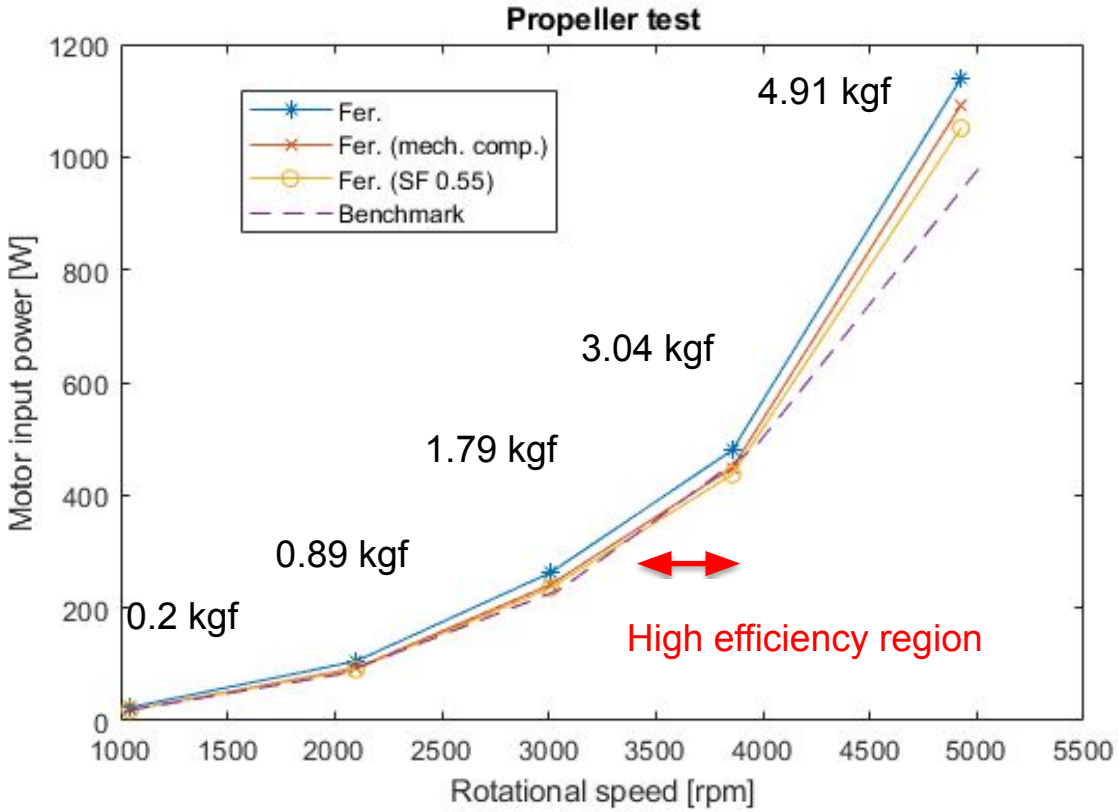

Motor Controls Research at NCSU

- Robust finite-set model predictive current controller (FS MPCC) with fixed switching (Modulated FS MPCC).
- Model-free predictive current control of dual three-phase motor drives using virtual vectors and no weight factors.
- Common-mode voltage suppression in dual three-phase motor drives.
- Compensation of PWM delays with double updates in modulated MPC drives.
- Computational cost reduction with simplified active vector pre-selection for predictive torque control of motor drives
- Parameter free sensorless control of PM motor drives

Model Free Predictive Current Controller (MFPCC)

Motivation for MFPCC

- Nonlinear motor parameters need to be determined through extensive FEA or Experiments
- Mutual cross-coupling between two windings complicates the conventional controller tuning process.
- Current harmonics causes motor losses and torque ripple

Single d-q Ultra-local Model for MFPCC

$$\mathrm{I}_{dq} = F + \alpha \mathrm{V}_{dq}$$

F accounts for the motor parameter dependent components and determined through an online observer

is a tunable constant.

$$V_{dq}^{*} = \frac{I_{dq}^{*(k+2)} - I_{dq}^{(k+1)}}{\alpha T_s} - \frac{\hat{F}^{(k+1)}}{\alpha}$$

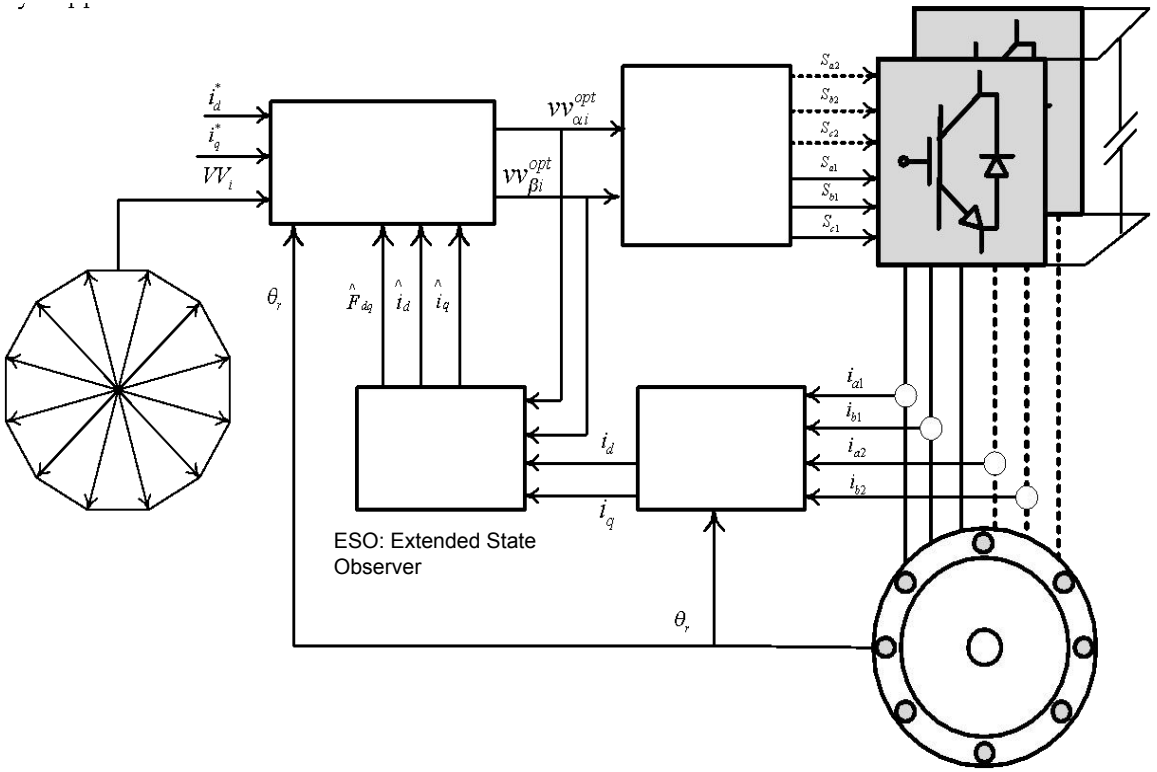

Block diagram of the MFPCC with Harmonic Current Reduction

*S. Agoro and I. Husain, "Model-Free Predictive Current and Disturbance Rejection Control of Dual Three-Phase PMSM Drives using Optimal Virtual Vector Modulation," IEEE Journal of Emerging and Selected Topics in Power Electronics; 2023

Experimental Results

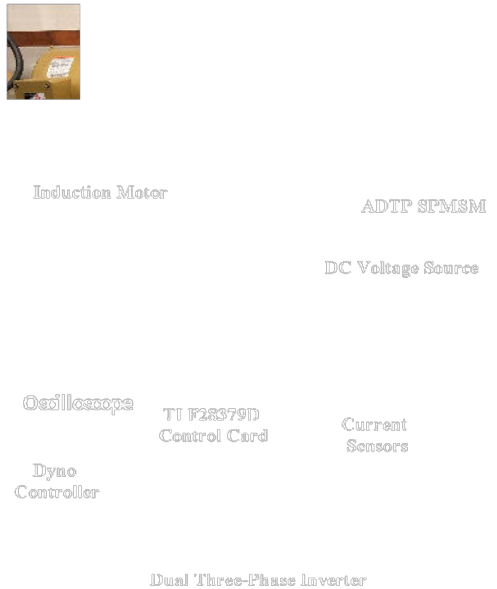

Test Bench

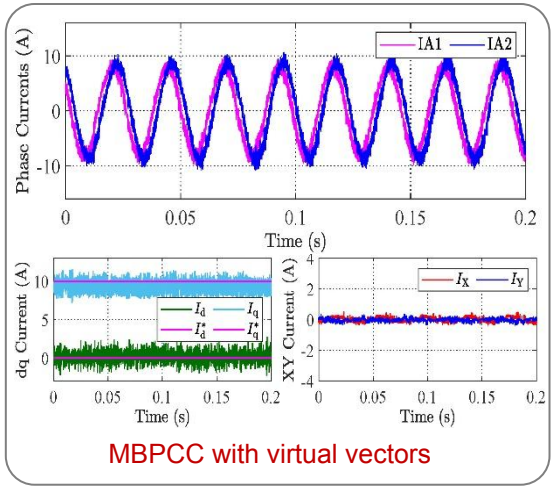

MBPCC with virtual vectors

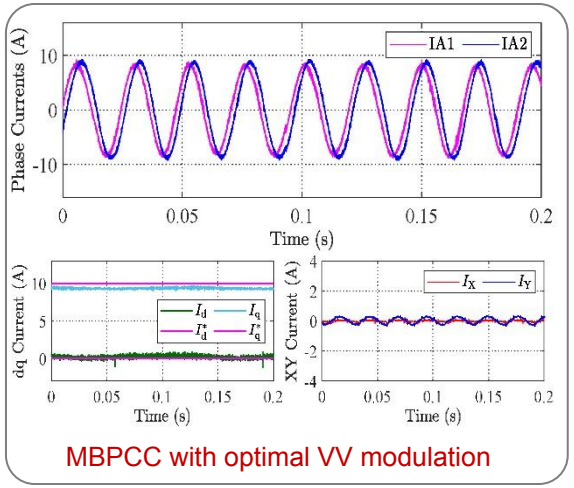

MBPCC with optimal VV modulation

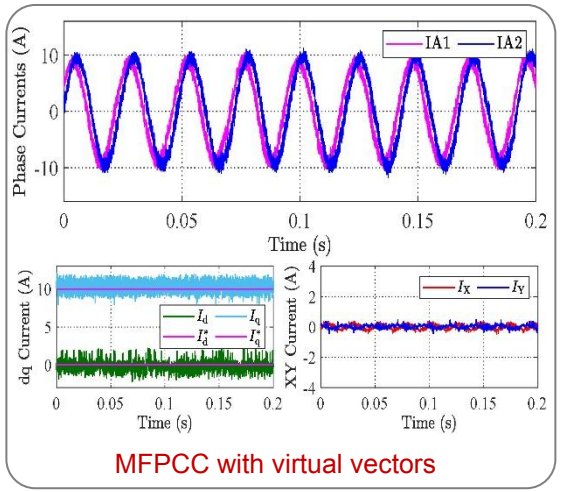

MFPCC with virtual vectors

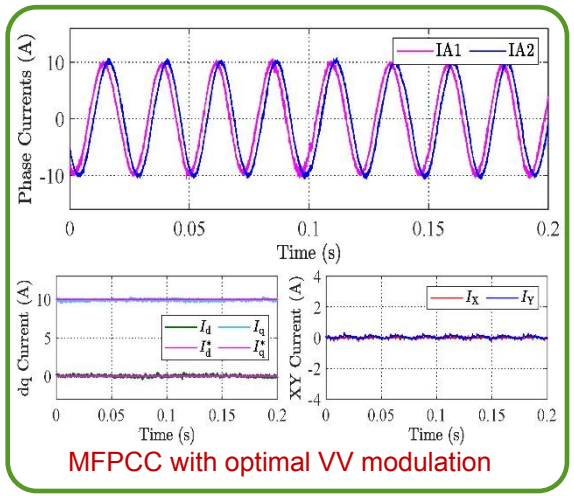

MFPCC with optimal VV modulation

Parameter Mismatch : $R = 0.3R_0,\ L = 1.25L_0,\ M = 1.25M_0,\ \psi_m = 1.25\psi_{mo}, \gamma = 2\gamma_0$

Experimental results of current control with mismatched parameters at 500 r/min and 10 A.

Summary

- Improved performance under mismatched conditions.
- The virtual vectors suppress xy harmonic currents without weight-based cost functions.
- Optimal virtual vector modulation reduces dq current ripple and phase distortion.
- Duty-cycle control results in a fixed switching operation.

Cross-Coupling Suppression in MABs

- Multi-Active Bridge (MAB) ports share a magnetic circuit which makes it a highly-coupled system.
- Suppression of cross-coupling effects is typically achieved through decoupling matrix.
- However, the design of decoupling matrix is highly sensitive to system parameters and operating conditions, and complexity increases with the number of ports.

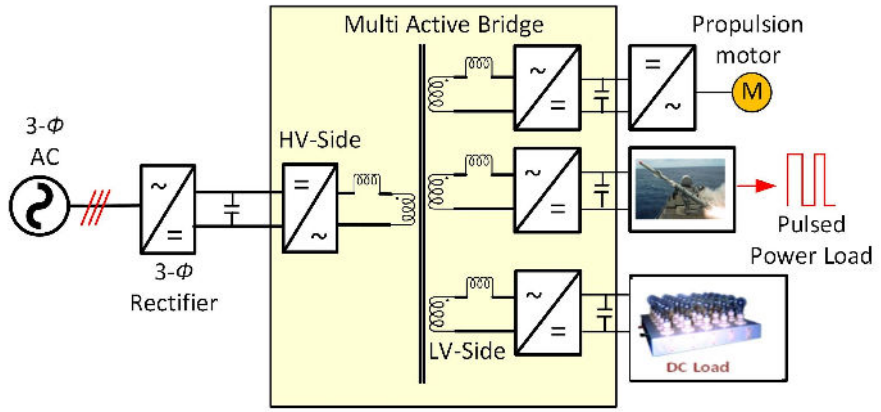

Multi-Active Bridge

Proposed ULM for MAB Port-k

$$\Delta V_k^n = F_k^n + \eta_k^n \cdot (\phi_k^{n-1}[\pi - |\phi_k^{n-1}|])$$

F_k^n captures unmodeled dynamics including cross-coupling, η_k^n is a non-physical gain. η_k^n and F_k^n are obtained using RLS

Quadratic Solution for Optimal Phase Shift

$$\phi_k^{n+1} = \begin{cases} \pi/2 - \sqrt{\pi^2/4 - M_k}, & M_k \geq 0 \\ -\pi/2 + \sqrt{\pi^2/4 + M_k}, & M_k < 0 \end{cases}$$

$$M_k = \frac{V_{ref} - \hat{V}_k^{n+1} - F_k^n}{\eta_k^n}$$

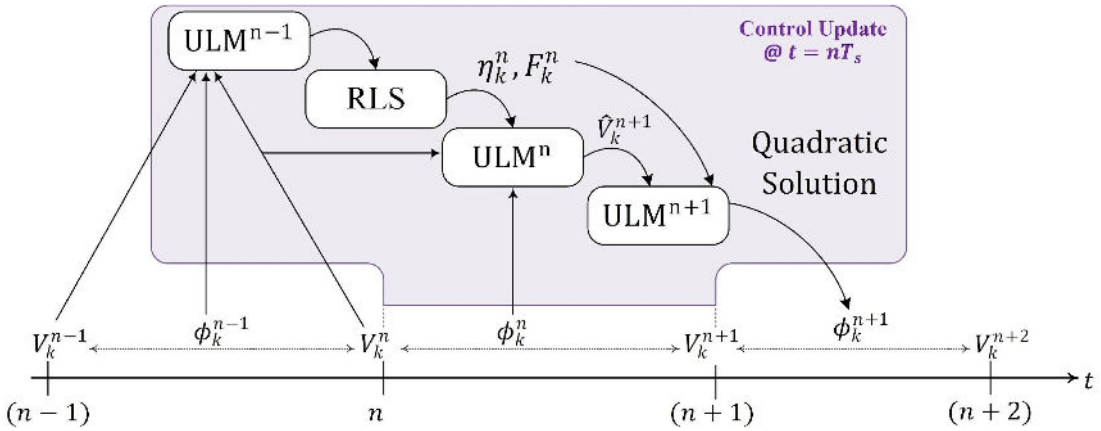

Control Implementation

*M. D. Alam, S. Osei Fobi, M. A. Awal, S. Lukic and I. Husain, "Computationally Scalable Model-Free Predictive Control of Multi-Active Bridge Converters with Inherent Power Flow Decoupling.